Clays and Clay Minerals, Vol. 61, No. 1, 11–25, 2013.

THE EFFECT OF ANTIMONATE, ARSENATE, AND PHOSPHATE ON THE TRANSFORMATION OF FERRIHYDRITE TO GOETHITE, HEMATITE, FEROXYHYTE, AND TRIPUHYITE

Ralph Michael Bolanz[1,*], Ulrich Bläss[1], Sonia Ackermann[1], Valerian Ciobotă[2], Petra Rösch[2], Nicolae Tarcea[3], Jürgen Popp[2,3], and Juraj Majzlan[1]

[1] Institute of Geoscience, Friedrich-Schiller-University, Jena, Germany
[2] Institute of Physical Chemistry, Friedrich-Schiller-University, Jena, Germany
[3] Institute of Photonic Technology, Jena, Germany

Abstract—Iron oxides, typical constituents of many soils, represent a natural immobilization mechanism for toxic elements. Most iron oxides are formed during the transformation of poorly crystalline ferrihydrite to more crystalline iron phases. The present study examined the impact of well known contaminants, such as P(V), As(V), and Sb(V), on the ferrihydrite transformation and investigated the transformation products with a set of bulk and nano-resolution methods. Irrespective of the pH, P(V) and As(V) favor the formation of hematite (α-Fe_2O_3) over goethite (α-FeOOH) and retard these transformations at high concentrations. Sb(V), on the other hand, favors the formation of goethite, feroxyhyte (δ'-FeOOH), and tripuhyite ($FeSbO_4$) depending on pH and Sb(V) concentration. The elemental composition of the transformation products analyzed by inductively coupled plasma optical emission spectroscopy show high loadings of Sb(V) with molar Sb:Fe ratios of 0.12, whereas the molar P:Fe and As:Fe ratios do not exceed 0.03 and 0.06, respectively. The structural similarity of feroxyhyte and hematite was resolved by detailed electron diffraction studies, and feroxyhyte was positively identified in a number of the samples examined. These results indicate that, compared to P(V) and As(V), Sb(V) can be incorporated into the structure of certain iron oxides through Fe(III)-Sb(V) substitution, coupled with other substitutions. However, the outcome of the ferrihydrite transformation (hematite, goethite, feroxyhyte, or tripuhyite) depends on the Sb(V) concentration, pH, and temperature.

Key Words—Antimony, Arsenic, Ferrihydrite, Feroxyhyte, Goethite, Hematite, Iron Oxides, Phosphorous, Transformation, Tripuhyite.

INTRODUCTION

Iron oxides are omnipresent constituents of most soils and count as important sinks for heavy metals and toxic elements (*e.g.* Ackermann *et al.*, 2009). Amongst the iron oxides, poorly crystalline 2-line ferrihydrite (referred to hereafter as ferrihydrite) is the initial secondary iron oxide formed during the weathering of primary iron minerals (Loan *et al.*, 2005). Ferrihydrite is generally considered to be an intermediate step in the formation of well crystallized iron oxides, such as goethite (α-FeOOH) and hematite (α-Fe_2O_3) (Cudennec and Lecerf, 2006). The outcome of the ferrihydrite transformation depends on temperature, pH, and abundance of foreign ions (*e.g.* Cornell *et al.*, 1987; Nagano *et al.*, 1994; Paige *et al.*, 1996, 1997; Shaw *et al.*, 2005; Cudennec and Lecerf, 2006; Das *et al.*, 2011a, 2011b). The most common products of the ferrihydrite transformation are goethite and hematite (Cornell and Schwertmann, 2003). Near or at the surface of the Earth both goethite and hematite are the two most stable iron oxides (Cornell and Schwertmann, 2003; Das *et al.*, 2011b). Although goethite and hematite can be formed simultaneously by ferrihydrite transformation (Das *et al.*, 2011b), conditions which are favorable for goethite are unfavorable for hematite and *vice versa* (Schwertmann and Murad, 1983). The transformation of ferrihydrite to goethite is thought to be a process in which ferrihydrite dissolves and goethite is formed by nucleation/crystallization from bulk solution (Schwertmann and Murad, 1983; Blesa and Matijevic, 1989; Cornell and Schwertmann, 2003). Hematite, on the other hand, is formed topotactically through atomic solid-solid rearrangement within the ferrihydrite matrix (Schwertmann and Murad, 1983; Johnston and Lewis, 1983; Cudennec and Lecerf, 2006; Cornell and Schwertmann, 2003). Because of these two different competing formation mechanisms (Schwertmann and Fischer, 1966), one could speculate that any parameter which leads to the stabilization of ferrihydrite favors the formation of hematite, whereas any parameter leading to the dissolution of ferrihydrite favors goethite formation. The first of these parameters is temperature. Elevated temperatures result in the aggregation of ferrihydrite particles (Fischer and Schwertmann, 1975) and lead to dehydration, which favors the formation of hematite (Cornell and Schwertmann, 2003; Cudennec and Lecerf,

* E-mail address of corresponding author:
ralph.bolanz@uni-jena.de
DOI: 10.1346/CCMN.2013.0610102

2006). The second parameter is pH. At room temperature, ferrihydrite is least soluble at pH 7–8 (Schwertmann and Murad, 1983), where goethite formation has its minimum and hematite is favored. Conversely, goethite formation from ferrihydrite has its maximum at pH 12 in alkaline media and pH 4 in acidic media at room temperature (Schwertmann and Murad, 1983). The third notable parameter is the abundance of foreign ions during the transformation process, which can affect the transformation rate and cause variations in the transformation products (for summaries see Jambor and Dutrizac (1998) and Cornell and Schwertmann (2003)).

The focus of the present study was the transformation of ferrihydrite in the presence of P(V), As(V), and Sb(V). In aqueous solution, P(V) and As(V) are both coordinated tetrahedrally by four oxygen atoms and show, at pH 4–12, the same species (H_2P/AsO_4^-, HP/AsO_4^{2-}, and P/AsO_4^{3-}) (Guan *et al.*, 2009). Sb(V), however, displays from pH 4–12 only one dominant species, $Sb(OH_6)^-$ (Filella *et al.*, 2002). In the presence of phosphate, the solubility (Majzlan, 2011) and consequently the transformation rate of ferrihydrite is reduced (Paige *et al.*, 1997), and aggregation of colloidal iron oxide particles is observed (He *et al.*, 1996), which leads to a preferred formation of hematite (Paige *et al.*, 1997). Like phosphate, arsenate favors the aggregation of ferrihydrite, decreases the transformation rate, and promotes the formation of hematite over goethite (Paige *et al.*, 1996).

P(V), As(V), and Sb(V) may occur together in Sb mine tailings and compete for the same adsorption sites on the surfaces of the more abundant minerals, especially ferrihydrite or its transformation products, goethite and hematite. The present study, therefore, examined the transformation of ferrihydrite into other, more crystalline iron oxides in the presence of antimonate, and compared the results with those for phosphate- and arsenate-doped ferrihydrite, transformed under the same conditions. To the authors' knowledge, no comparable transformation experiments have ever been performed with antimonate. The newly formed products were characterized using an array of bulk and nano-resolution methods.

MATERIALS AND METHODS

Two-line ferrihydrite was synthesized after Schwertmann and Cornell (2000). A mass of 10.1 g $Fe(NO_3)_3{\cdot}9H_2O$ (Alfa Aesar, Ward Hill, Massachusetts, USA) was dissolved in 200 mL of deionized water and transformed into 2-line ferrihydrite by adding 45 mL of 5 M potassium hydroxide (Merck, Darmstadt, Germany) solution under constant stirring. The suspension was adjusted to 490 mL with deionized water, resulting in an end-point pH of ~13. The suspension was then adjusted to 500 mL with deionized water. The resulting brown aggregates (flocs) settled after a few minutes in suspension and showed a dry weight of ~7 g (air-dried). This ferrihydrite slurry was immediately adjusted to the desired pH (4, 7, or 12) by adding nitric acid (65%) (J.T. Baker, Center Valley, Pennsylvania, USA) and doped with pre-selected volumes of a 15 mM solution of potassium hexahydroxoantimonate (Merck, Darmstadt, Germany) for Sb(V), arsenic pentoxide (Alfa Aesar, Ward Hill, Massachusetts, USA) for As(V), and potassium dihydrogen phosphate (Merck, Darmstadt, Germany) for P(V). Previous studies indicated that nitrate does not significantly interfere with the adsorption of P(V), As(V), and Sb(V) onto amorphous $Fe(OH)_3$ (Álvarez-Benedí *et al.*, 2005; Tighe *et al.*, 2005). The ferrihydrite synthesized was, therefore, unwashed in order to maintain the calculated Fe concentration and, thus, to keep the Fe to P/As/Sb ratio constant. The volumes of the doping solutions were calculated to arrive at the P(V)/As(V)/Sb(V) molarity of 0 mM, 0.225 mM, 0.750 mM, 2.250 mM, and 6.000 mM after adjusting to 500 mL with deionized water. After bringing the volume to ~490 mL, the pH was checked and adjusted again if necessary by adding nitric acid (65%) or 5 M potassium hydroxide solution and the volume finally brought to 500 mL with deionized water. The samples were then stored at 70ºC for up to 16 days and sample aliquots were taken every second day, washed, air-dried, and sealed in glass vials. The synthesis of ferrihydrite involved high pH conditions under which Si may be mobilized into the aqueous solutions. For this reason polyethylene (PE) containers were used exclusively during this work, rather than glassware.

A second series of ferrihydrite samples was synthesized as described above. In this series, ferrihydrite was doped at pH 4 in smaller concentration steps with molar Sb:Fe ratios of 0.000–0.080 in steps of 0.005, 0.090, 0.100, and 0.300; 0.300–0.500 in steps of 0.025, and 0.500–1.000 in steps of 0.100. The doped ferrihydrite was again incubated for 16 days at 70ºC, washed, air-dried, and sealed in glass vials.

Several reference compounds were synthesized for Raman spectroscopy measurements. The hematite (α-Fe_2O_3) reference was synthesized by transforming 2-line ferrihydrite at pH 4 and 70ºC in aqueous solution for 16 days. The sample was washed, air-dried, and sealed in a glass vial. Pure feroxyhyte (δ'-FeOOH) was synthesized after Schwertmann and Cornell (2000). A mass of 5.96 g $FeCl_2{\cdot}4H_2O$ was dissolved in 300 mL of deionized water and adjusted to pH 8 with 5 M NaOH solution. 40 mL of H_2O_2 (30%) was added quickly and the pH was again adjusted to 8. The product was washed, air-dried, and sealed in glass vials. Tripuhyite reference 1 was synthesized using a modified version of the Diemar *et al.* (2009) recipe. A solution of 0.1 M $Fe_2(SO_4)_3{\cdot}H_2O$ (Sigma-Aldrich) was mixed with a 0.1 M $KSb(OH)_6$ (Merck, Darmstadt, Germany) solution at a ratio of 1:2.

The brown precipitate was refluxed for three days at 100ºC, washed, air-dried, and sealed in a glass vial. Tripuhyite reference 2 was synthesized using a modified version of the Martinelli *et al.* (2004) recipe. Hematite, synthesized as described above, was mixed with Sb_2O_5 (Alfa Aesar, Ward Hill, Massachusetts, USA) and heated in a sintered corundum crucible for 24 h at 600ºC, followed by 48 h at 900ºC and cooled over 12 h to 25ºC. Immediately after the synthesis, tripuhyite was washed, air-dried, and sealed in a glass vial. All reference compounds were analyzed and checked for impurities by X-ray diffraction (XRD).

The pH was measured with a pH100 pH meter (VWR, Radnor, Pennsylvania, USA), which was calibrated with a pH 6.86 (HANNA Instruments, Woonsocket, Rhode Island, USA) and a pH 4.00 buffer solution (HANNA Instruments, Woonsocket, Rhode Island, USA) according to the calibration procedure.

Elemental composition (P, As, Sb, and Fe) was determined by inductively-coupled plasma optical emission spectrometry (ICP-OES) using a Quadrupol-ICP-MS X SeriesII (ThermoFisher Scientific, Bremen, Germany) with a charge-coupled device (CCD) detector.

Powder XRD patterns were collected using a Bruker D8 Advance DaVinci diffractometer (Karlsruhe, Germany), employing CuKα radiation (λ = 1.54058 Å). The patterns were collected at room temperature between 5 and 90º2θ, with a step size of 0.02º2θ and a collection time of 1 s/step. The proportions of the phases in the samples were extracted from the XRD patterns. To check the procedure, a standard was prepared containing 25 wt.% ferrihydrite, 25 wt.% goethite, 25 wt.% hematite, and 25 wt.% feroxyhyte. In order to quantify the area (intensity) of the following reflections, the program *Fityk* 0.9.8 (Wojdyr, 2010) was used: ferrihydrite 33.90º2θ, goethite 21.37º2θ (101), hematite 24.15º2θ (012), and feroxyhyte 35.13º2θ (100). The intensities obtained were normalized for hematite and feroxyhyte to 100% and all the intensities were weighted by I/I_{cor} values, taken from the Crystallography Open Database (COD) (Downs and Hall-Wallace, 2003; Gražulis *et al.* 2009, 2012); ferrihydrite 1.03 (COD 9012761), goethite 2.92 (COD 9002158), hematite 4.82 (COD 1011267), and feroxyhyte 2.27 (COD 1008762). This method enabled the quantification of all phases in the samples with an inaccuracy of <5 wt.% for the standard prepared. The incorporation of elements heavier than iron (*e.g.* As, Sb) into the iron oxides can affect the XRD peak intensities, and must be taken into account.

The morphology and grain size for goethite and hematite were examined by scanning electron microscopy (SEM) using a Carl Zeiss ULTRA PLUS FE-SEM (Oberkochen, Germany) operating at 20 kV with an Inlens SE-detector. Several milligrams of air-dried sample were distributed over a conductive carbon pad with adhesive properties (PLANO, Wetzlar, Germany). As all the samples studied were <1 μm across, the samples were not coated with carbon which could have masked the morphological characteristics.

Morphological characteristics, grain size, and electron diffraction of feroxyhyte samples were studied by transmission electron microscopy (TEM) using a LEO922 OMEGA instrument (Carl Zeiss, Oberkochen, Germany) operating at 200 kV with an in-column Omega filter and energy dispersive X-ray (EDX) detector. The feroxyhyte sample was suspended in ethanol, placed on a Lacey copper grid, and air dried to prepare it for analysis.

The specific surface area of selected transformation products was determined using the Brunauer-Emmet-Teller (BET) method (Brunauer *et al.*, 1938) with a Quantachrome Autosorb (Odelzhausen, Germany) automated gas sorption system. About 0.2 g of the sample was outgassed at 70ºC for 2−7 h and measured using evaporated liquid N_2 as the adsorbate gas.

Raman analyses of the iron oxides were performed using a commercial micro-Raman setup (HR LabRam inverse system, Jobin Yvon Horiba) (Kyoto, Japan). Raman scattering was excited by a frequency doubled Nd:YAG laser at a wavelength of 532 nm with a laser power of ~20 μW incident on the sample. The low laser power was selected to prevent alteration of the sample. The laser beam was focused on the sample by means of a Leica PLFluoar ×100/0.75 microscope objective lens down to a spot diameter of ~0.7 μm. The dispersive spectrometer had an entrance slit of 100 μm, a focal length of 800 mm, and was equipped with a grating of 300 lines/mm. The Raman scattered light was detected by a Peltier-cooled CCD detector. The integration times for one Raman spectrum ranged from 60 to 1000 s.

RESULTS

Morphology and surface area

The ferrihydrite samples synthesized had a specific surface area of 252 m^2/g, in good agreement with other studies (Hansen *et al.*, 1994; Larsen and Postma, 2001). Goethite synthesized at pH 12 consisted of acicular crystals 250−1750 nm long and 80−200 nm in diameter with a specific surface area of 25 m^2/g, whereas hematite synthesized at pH 4 displayed rhombohedral crystals with a particle size of 35−260 nm and a specific surface area of 30 m^2/g. These values are consistent with the literature (Cornell and Schwertmann, 2003). Feroxyhyte samples formed at pH 4 and Sb(V) concentrations of 6 mM exhibited rhombohedral crystals with a size of 10−30 nm and a specific surface area of 94 m^2/g, which is less than the given values for Sb-free feroxyhyte of 140−240 m^2/g (Carlson and Schwertmann, 1980).

Products of transformation experiments (XRD, Raman spectroscopy, and TEM)

In the transformation experiments (summarized in Figure 1) the phases produced in the runs were color-

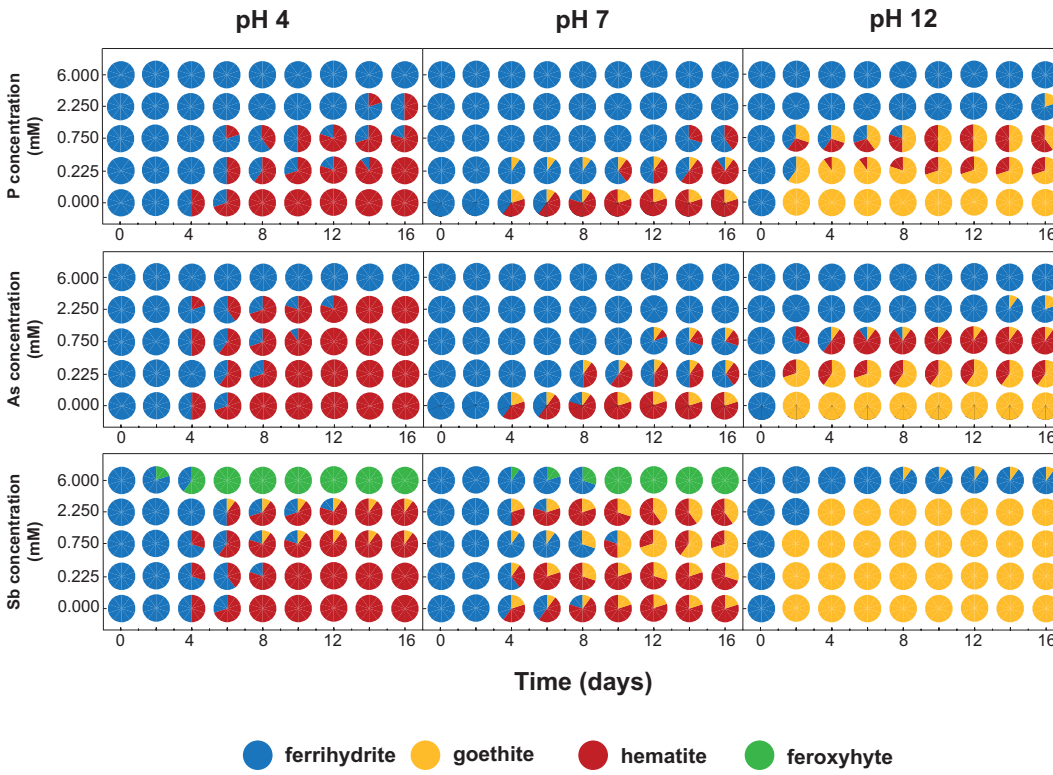

Figure 1. Iron oxide speciation and quantification for P-, As-, and Sb-doped ferrihydrite and subsequently formed transformation products.

coded and the pie charts show the quantitative proportions of the phases. The results were sorted according to the two principal variables used in the runs, starting pH of the solution and the molarity of a pentavalent cation, either P(V), As(V), or Sb(V). Temperature was kept constant at 70ºC in all runs.

Under acidic conditions (pH 4), in the absence of P(V), As(V), or Sb(V), and at 70ºC, ferrihydrite transformed completely to hematite within 8 days (Figure 1), an expected result, considering the preferred formation of hematite at elevated temperatures (Cornell and Schwertmann, 2003, p. 389). In the presence of P(V) and As(V), the transformation rate generally declined with increasing concentrations, to a complete inhibition at 6.00 mM P(V) or As(V). The presence of Sb(V), however, led to a more complex transformation behavior. At low Sb(V) concentrations (0.225 mM), the transformation to hematite was slightly retarded. With increasing Sb(V) concentrations, goethite appeared in addition to hematite and the transformation rate was diminished. At 6.00 mM Sb(V), surprisingly, the transformation rate suddenly increased with feroxyhyte as the only crystalline transformation product after 6 days.

At neutral pH (7), the transformation of pure ferrihydrite took 12 days and yielded a mixture of 70 wt.% hematite and 30 wt.% goethite. P(V) and As(V) retarded the transformation process significantly and caused a complete inhibition at concentrations of 2.25 mM and above. In the presence of Sb(V), the transformation was again not only affected by retardation but, just as at pH 4, the presence of Sb(V) seemed to favor goethite, but in the presence of 6.00 mM Sb(V) the ferrihydrite was converted almost completely to feroxyhyte with traces of hematite (the latter detected only by Raman spectroscopy).

Under alkaline conditions (pH 12) and in the absence of 'foreign' ions, ferrihydrite transformed almost completely within 2 days to goethite, with traces of hematite (detected by Raman spectroscopy). No changes in composition were observed until day 16, when the experiment was terminated. These observations are consistent with the results of Schwertmann and Murad (1983), Nagano *et al.* (1994), and Cudennec and Lecerf (2006).

P(V) and As(V) favored hematite formation over goethite, and retarded the transformation process significantly at concentrations of 2.25 mM. At concentrations of 6.00 mM only traces of hematite were detected by Raman spectroscopy. In the presence of Sb(V), ferrihydrite transformed almost undisturbed to goethite. Only at concentrations of 6.00 mM Sb(V) was a retarding effect observed. The main transformation product was goethite with traces of hematite (detected by Raman spectroscopy).

Table 1. Iron oxide speciation by Raman spectroscopy from selected ferrihydrite transformation products. fh: ferrihydrite, goe: goethite, hem: hematite, and fx: feroxyhyte. The asterisk marks components occurring in trace amounts which were not detected by XRD.

Additive	Concentration	pH4	pH7	pH12
P^{5+}	high (6. mM)	fh/hem*	fh	fh/hem*
	low (0.75 mM)	fh/hem	fh/hem	goe/hem
	free (0 mM)	hem	goe/hem	goe/hem*
As^{5+}	high (6 mM)	fh/hem*	fh	fh/hem*
	low (0.75 mM)	fh/hem	fh/goe/hem	goe/hem
	free (0 mM)	hem	goe/hem	goe/hem*
Sb^{5+}	high (6 mM)	fx	fx/hem*	fh/goe/hem*
	low (0.75 mM)	goe/hem	goe/hem	goe
	free (0 mM)	hem	goe/hem	goe/hem*

Raman spectroscopy is a powerful tool for mineral identification (Dörfer *et al.*, 2010; Ciobotă *et al.*, 2012), especially for iron oxides (Hanesch, 2009). For this reason, selected samples were analyzed by Raman spectroscopy. The Raman spectra (summarized in Table 1) confirmed the XRD measurements and complemented them by identifying iron oxide species occurring in trace amounts only.

Because of the poor crystallinity of feroxyhyte, this phase was also characterized by TEM. Several selected-area electron diffraction (SAED) patterns of single feroxyhyte crystals were collected (Figure 2). Feroxyhyte formed rhombohedral crystals 10−30 nm across and with sharp diffraction spots. Despite the sensitivity of feroxyhyte (fx) to the electron beam and its small size, one crystal was tilted carefully by up to ~18º along the $[110]_{fx}$ axis from the $[1\bar{1}1]_{fx}$ zone to the $[2\bar{2}1]_{fx}$ zone. These measurements confirmed the 3D consistency with the feroxyhyte lattice.

Chemical composition of the transformation products (ICP-OES)

The elemental composition of all 405 runs (shown in Figure 1) is summarized in Figure 3. A direct comparison between the different loadings (P(V), As(V), Sb(V)) is complex, considering that different anions lead to different ratios amongst the transformation products and retard the transformation at different rates.

At pH 12 and concentrations of up to 0.750 mM, P(V) and As(V) led to goethite + hematite mixtures which were free of untransformed ferrihydrite. At 0.750 mM, molar P:Fe and As:Fe ratios of 0.0024 and 0.0068, respectively, were observed. Higher P(V) and As(V) concentrations (2.250−6.000 mM) led to ferrihydrite as the dominant phase, showing significantly larger molar P:Fe and As:Fe ratios of 0.012 and 0.024, respectively. In the presence of Sb(V), pure goethite was even formed at concentrations of 2.250 mM. These goethite samples showed molar Sb:Fe ratios of 0.034. At Sb(V) concentrations of 6.000 mM,

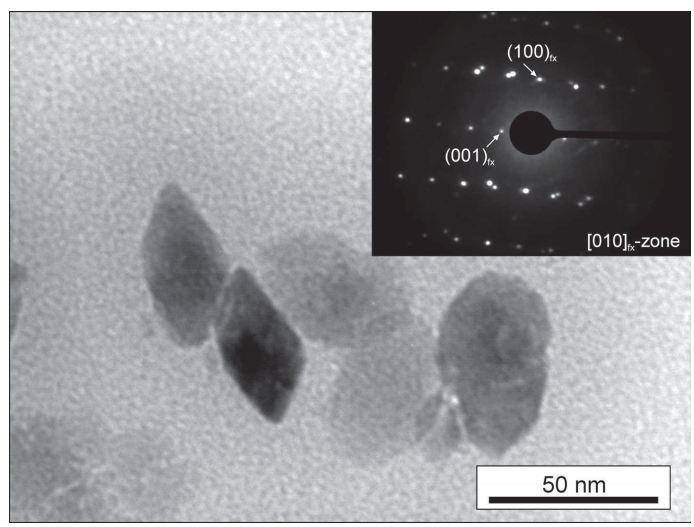

Figure 2. Bright-field TEM image and corresponding selected area electron diffraction pattern (inset) of that area showing the rhombohedral shape and the sharp diffraction spots of feroxyhyte.

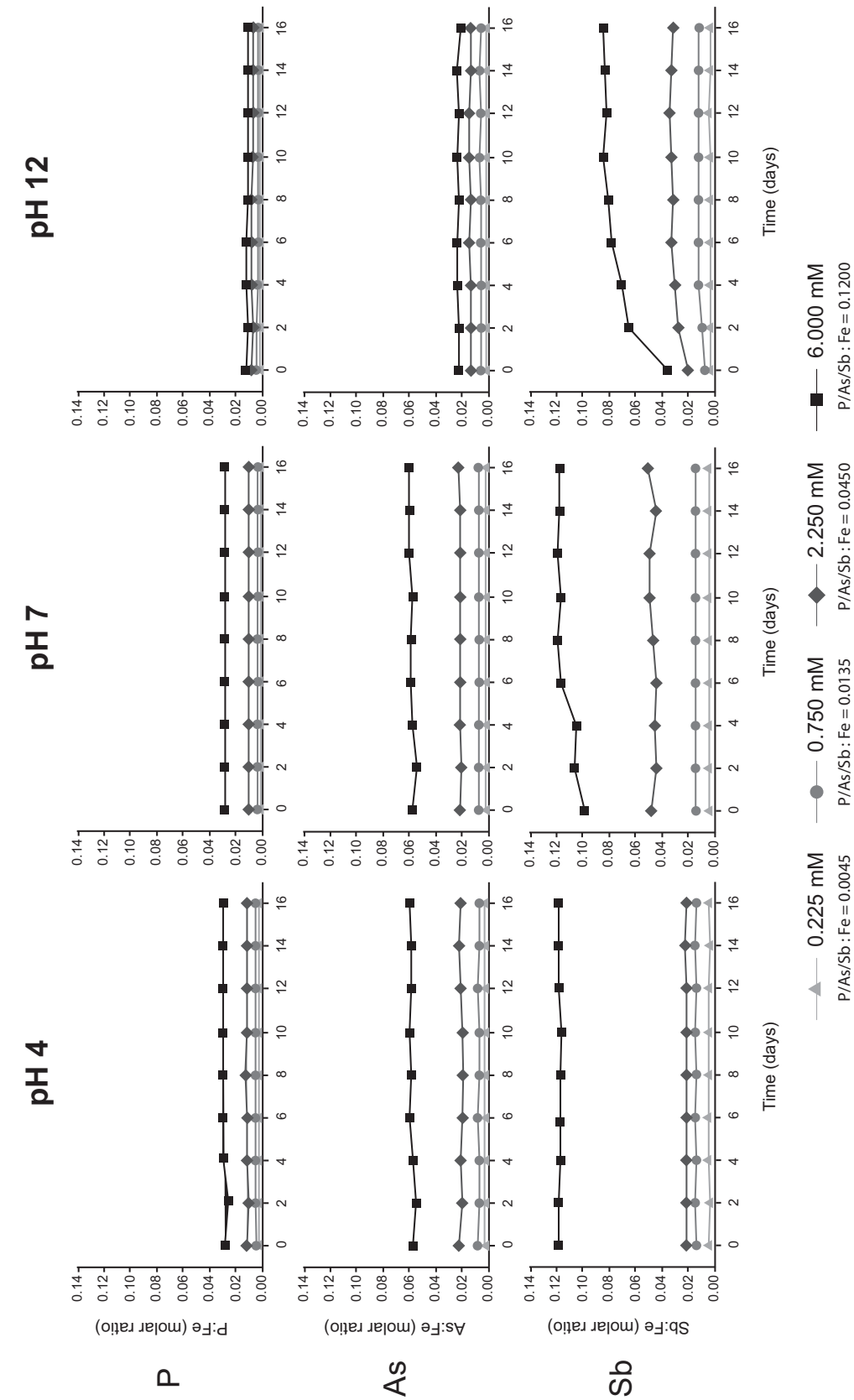

Figure 3. Chemical composition of the transformation products given as molar ratios of P, As, and Sb *vs.* Fe. The molar starting ratios of P/As/Sb:Fe are given for each concentration step.

goethite formed but ferrihydrite remained as the dominant phase until day 16, when the experiment was terminated. The goethite + ferrihydrite mixtures displayed molar Sb:Fe ratios of 0.085.

At pH 7, neither P(V)- nor As(V)-doped ferrihydrite transformed completely. Samples doped with P(V) revealed a maximum molar P:Fe ratio of 0.028, whereas As(V)-doped samples showed a maximum molar As:Fe ratio of 0.060. Ferrihydrite doped with Sb(V), however, displayed a maximum molar Sb:Fe ratio of 0.052 (at 2.25 mM) for the goethite + hematite mixtures and 0.121 (at 6.00 mM) for feroxyhyte.

At pH 4, P(V) and As(V) revealed the highest concentrations in untransformed ferrihydrite (at 6.00 mM) with molar P:Fe and As:Fe ratios of 0.029 and 0.060, respectively. Again, the highest Sb(V) concentrations were found in feroxyhyte with molar Sb:Fe ratios of 0.120. Surprisingly, the goethite + hematite mixtures (formed at 2.25 mM Sb) contained not only less Sb(V) than in similar mixtures formed at pH 7, but also less than in goethite formed at pH 12.

Transformations at increasing Sb:Fe ratios

During the ferrihydrite transformations at pH 4 and 7, an increase in goethite abundance and the formation of feroxyhyte was observed. In order to investigate these two changes in transformation products and to evaluate the stability of feroxyhyte at even higher Sb:Fe ratios, a second experiment at smaller concentration steps was performed. The conditions of temperature at 70ºC and 16 days of transformation time were maintained for all samples. Selected XRD patterns of the experiment are shown in Figure 4.

In the absence of Sb(V) (molar Sb:Fe ratio of 0.000) and pH 4, hematite was the only transformation product. With increasing Sb(V) concentrations, the formation of goethite (goe) was indicated by a growing (101) peak at 21.15º2θ. The increase in intensity of the $(101)_{goe}$ peak was coupled with an increase of its full width at half maximum value (FWHM), and hence, a decrease in the crystallinity of goethite. Hematite was also affected by increasing Sb(V) concentrations, showing decreasing intensities and an increasing FWHM of its peaks. However, the peaks ascribed to hematite did not decrease equally in intensity. From the dominant hematite peaks, (102), (104), and (024) decreased strongly in intensity, whereas (110), (113), (116), and (300) decreased far less. Simultaneously, the hematite peaks (006) and (226) increased in intensity. The remaining peaks at a molar Sb:Fe ratio of 0.300 correspond well with the feroxyhyte peaks {100}, {002}, {101}, {102}, {110}, and {202}.

With further increasing Sb(V) concentrations, the FWHM of the feroxyhyte peaks increased. At molar Sb:Fe ratios of 0.600−1.000, the only crystalline ferrihydrite transformation product was the iron antimonate, tripuhyite ($FeSbO_4$).

As both feroxyhyte and tripuhyite are poorly crystalline transformation products, the XRD results were confirmed by Raman spectroscopy (selected spectra are shown in Figure 5). Sample pH4Sb6.000 was the product of ferrihydrite transformed at pH 4, 70ºC, and Sb(V) concentrations of 6.000 mM, with an aging time of 16 days. The Raman spectrum confirmed feroxyhyte as the only transformation product with impurities of KNO_3 from the ferrihydrite synthesis. Sample pH7Sb6.000 was formed under the same conditions, but at pH 7 instead of pH 4. In this case feroxyhyte was accompanied by traces of hematite and again some minor KNO_3 impurities. At a molar Sb:Fe ratio of 0.600 (sample pH4Sb:Fe0.600), no feroxyhyte was formed but tripuhyite instead. This tripuhyite was poorly crystalline, which reduced the quality of the Raman spectrum considerably. In comparison to tripuhyite reference 1, synthesized following the method of Diemar *et al.* (2009), only minor similarities could be observed with sample pH4Sb:Fe0.600, *i.e.* mainly the band at ~620 cm^{-1}. Tripuhyite reference 2, synthesized following the method of Martinelli *et al.* (2004), was in better agreement with the sample. However, the bands at ~740 cm^{-1} and ~500 cm^{-1} were not distinctive, and the band at ~420 cm^{-1} was missing. Furthermore, both tripuhyite reference compounds were clearly identified by XRD, although the Raman spectra showed only minor similarities between them (see Figure 5). The Raman spectra of feroxyhyte, therefore, agree well with the XRD results. The Raman spectra of tripuhyite, however, showed considerable differences between the sample (pH4Fe:Sb0.600) and the reference compounds (prepared using two different methods), and also between the reference compounds themselves. The poor crystallinity of the nano-sized tripuhyite in sample pH4Fe:Sb0.600 could lead to phonon-confinement effects, often observed in nano-sized crystallites (*e.g.* Georgescu *et al.*, 2012), causing the observed band shifts in the Raman spectrum.

DISCUSSION

Maximum adsorption capacities

With the measured specific surface area of the transformation products and the necessary surface area for the adsorption of P(V), As(V), and Sb(V) complexes taken from the literature, maximum adsorption capacities for a simple adsorption model could be calculated.

The specific surface area of ferrihydrite should be handled with care, because it is highly variable and can fluctuate between 100 and 700 m^2/g (Cornell and Schwertmann, 2003). Considering that the structure and chemical formula is still under debate (Michel *et al.*, 2007; Jambor and Dutrizac, 1998), adsorption calculations for ferrihydrite bear a significant uncertainty. The area required for the adsorption of one phosphate ion to the ferrihydrite surface varies between 0.33 and 0.62 nm^2 (Ryden *et al.*, 1977; Borggaard *et al.*, 2005; Gimsing and

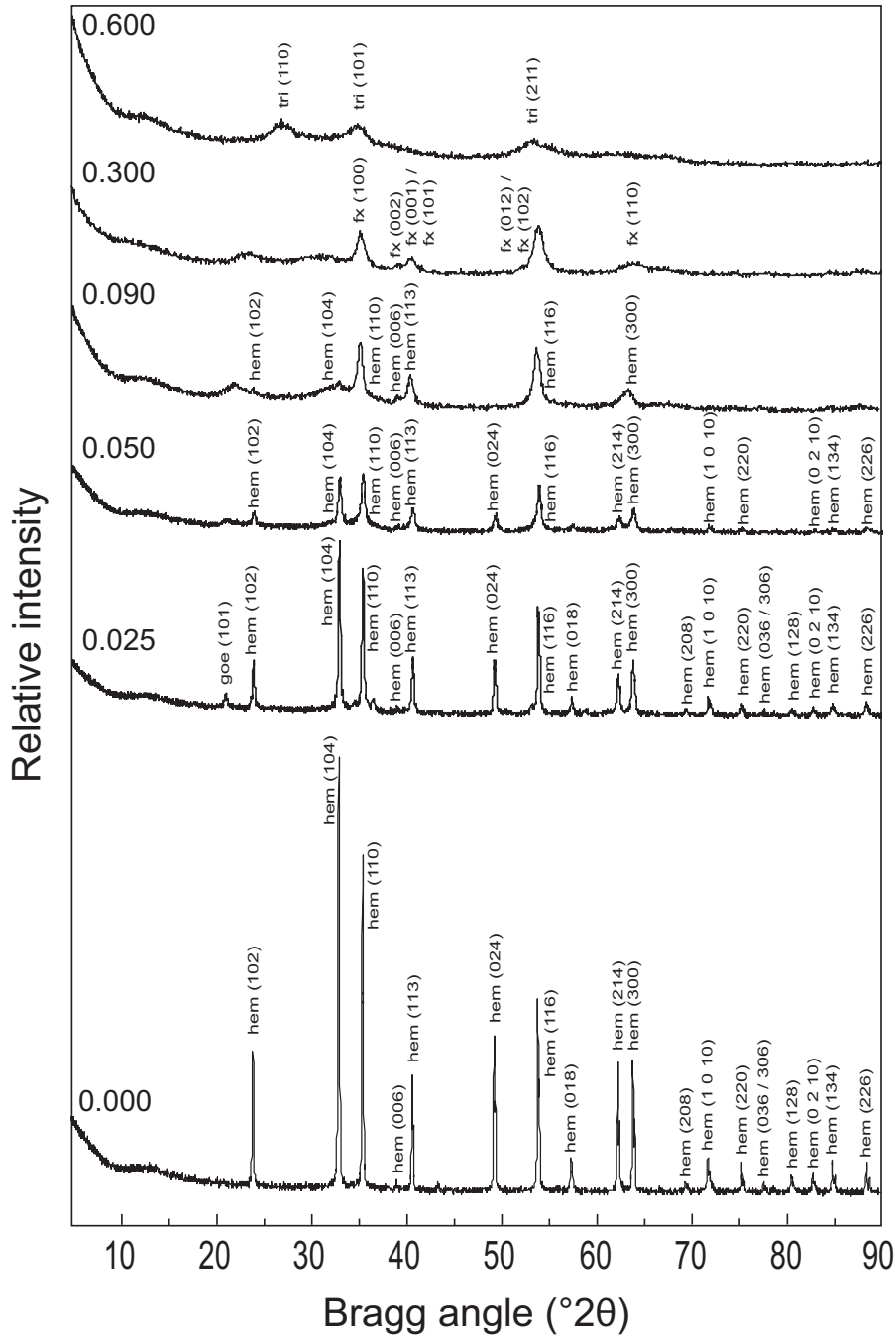

Figure 4. Ferrihydrite transformation in the presence of increasing Sb(V) concentrations. The numbers in front of each pattern indicate the molar Sb:Fe ratio. hem: hematite, goe: goethite, fx: feroxyhyte, tri: tripuhyite. All experiments were performed at pH 4 and with an aging time of 16 days.

Borggaard, 2007; Arai and Sparks, 2001) and for arsenate 0.40 nm^2 (Zhu *et al.*, 2011). These values led to a calculated maximum adsorption capacity for phosphate and arsenate of 39.27 (5.03 μmol/m^2) and 78.44 mg/g (4.18 μmol/m^2), respectively. To the authors' knowledge, no information about the area taken by one antimonate ion at the surface of ferrihydrite is available.

For goethite, the reported areas for an adsorbed phosphate ion are 0.61–0.66 nm^2 (Atkinson *et al.*, 1972; Barrow *et al.*, 1981; Torrent *et al.*, 1990; Borggaard *et al.*, 2005); those for an arsenate ion, 0.65–1.11 nm^2 (Salazar-Camacho and Villalobos, 2010; Wainipee *et al.*, 2010; Mamindy-Pajany *et al.*, 2011); and for an antimonate ion, 0.417 nm^2 (Leuz *et al.*, 2006). These

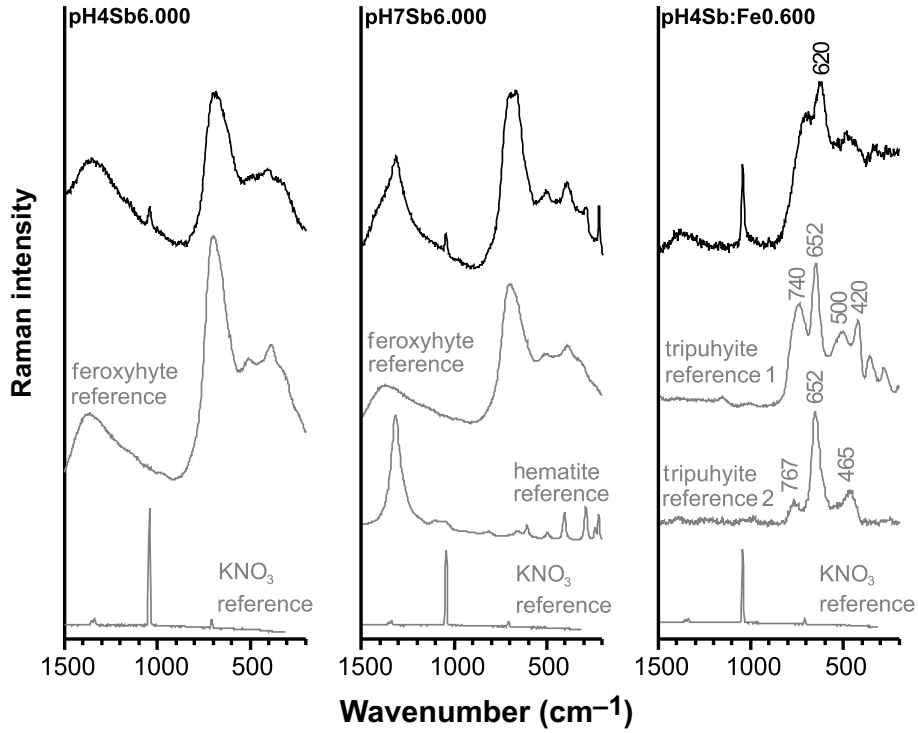

Figure 5. Selected Raman spectra of ferrihydrite transformations at increased Sb(V) concentrations. Sample 1 was transformed at pH 4, 70ºC, and Sb(V) concentration of 6.000 mM with an aging time of 16 days. Sample 2 was transformed under the same conditions, but pH 7 instead of pH 4. Sample 3 was transformed at a Sb:Fe molar ratio of 0.600 at pH 4, 70ºC, and 16 days of aging.

values led to a maximum adsorption capacity of goethite for P(V) of 2.11 mg/g (2.72 μmol/m^2), As(V) 4.79 mg/g (2.55 μmol/m^2), and Sb(V) 12.03 mg/g (3.95 μmol/m^2). Hematite is more complex with regard to its adsorption capacity as both morphology and grain size are very dependent on the synthesis conditions (Cornell and Schwertmann, 2003) and, therefore, adsorption capacity varies (Barron *et al.*, 1988; Torrent *et al.*, 1994). The area required for an adsorbed phosphate ion is between 0.40 and 0.61 nm^2 (Barron *et al.*, 1988; Colombo *et al.*, 1994; Torrent *et al.*, 1994; Gimsing and Borggaard, 2007); for an arsenate ion, 0.37 nm^2 (Mamindy-Pajany *et al.*, 2011); and for an antimonate ion, 0.780 nm^2 (Ambe, 1987). For hematite, maximum adsorption capacities for P(V) of 3.86 mg/g (4.15 μmol/m^2), As(V) 10.10 mg/g (4.49 μmol/m^2), and Sb(V) 7.78 mg/g (2.13 μmol/m^2) were reached. To the authors' knowledge, no comparable information for feroxyhyte is available.

The chemical composition of the transformation products indicates that the P(V) and As(V) contents were all below the calculated maximum adsorption capacities, except for hematite, which contained up to 27.35 mg As/g. For Sb(V), the highest concentrations occurred in feroxyhyte with 142.56 mg of Sb/g, followed by ferrihydrite with 110.30 mg of Sb/g. Unfortunately, no comparable literature values are available for Sb(V) adsorption for both minerals. Goethite contained 44.39 mg of Sb/g, significantly more than the calculated maximum adsorption capacity, whereas pure hematite was only present in a low-Sb(V) environment, remaining below the calculated adsorption capacity at 7.01 mg of Sb/g.

Considering the calculated maximum adsorption capacities, the Sb(V) loadings in the goethite samples are considerably greater than expected from a simple adsorption system. One could, therefore, speculate that Sb(V) is not only adsorbed to the surface of the goethite crystals but incorporated into their structure.

The validity of these calculated maximum adsorption capacities must be considered as a rough approximation. This model assumes a complete mononuclear, monodentate coverage of the whole specific surface area, not taking reactive adsorption sites, crystal morphology, or shielding of other ions into account. Furthermore, the adsorption to ferrihydrite, still without a widely accepted crystal structure or chemical composition, is poorly understood. The aggregates formed by ferrihydrite and the size of the single particles may have a significant impact on the adsorption behavior and, therefore, on the adsorption capacity. Hematite, on the other hand, has a well defined crystal structure and chemical composition, though the size of the crystallites and their habit depends heavily on the formation conditions. For ferrihydrite and hematite, therefore, adsorption densities from the literature may be insufficient for the calculation of maximum adsorption capacities. Adsorption capacities calculated from literature values are summarized graphically in Figure 6.

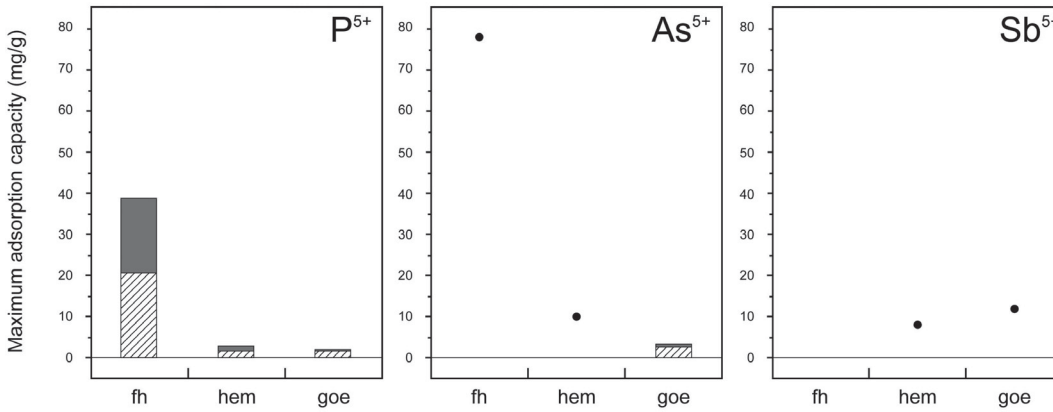

Figure 6. Graphical summary of the maximum adsorption capacities calculated from different literature values. The striped bars show the adsorption capacity that can be reached by every cited literature value. The gray bars indicate the uncertainty for the maximum adsorption capacity calculated from literature values. Dots indicate that only one literature value was available. fh: ferrihydrite, hem: hematite, goe: goethite.

Feroxyhyte or hematite

At increasing Sb(V) concentrations, the XRD patterns showed an apparent transition between hematite (α-Fe_2O_3) and feroxyhyte (δ'-FeOOH). The six indicative peaks of feroxyhyte (100), (002), (011/101), (012/102), (110), and (022/202), which can be seen in the powder XRD patterns, share the same 2θ positions as the hematite peaks (110), (113), (116), (300), (006), and (226), respectively. A problem arises when hematite and feroxyhyte coexist, because the powder XRD pattern is a linear combination of the patterns of both minerals, with a complete overlap of the feroxyhyte peaks with hematite peaks.

Therefore, all electron diffraction patterns of feroxyhyte were also cross-checked for indexing with a hematite (space group $R\bar{3}c$) model. The results showed that the lattice of feroxyhyte coincides completely with the lattice of hematite. All feroxyhyte indices can, therefore, be converted to hematite indices by a transformation of the lattice basis. The relation of the two lattices is given by the following transformation matrix:

$$\bar{h}_{\mathrm{hem}} = \bar{h}_{\mathrm{fx}} \cdot \mathbf{P} \qquad \text{with } \mathbf{P} = \begin{pmatrix} 1 & 1 & 0 \\ \bar{1} & 2 & 0 \\ 0 & 0 & 3 \end{pmatrix} \qquad (1)$$

The unit-cell volume of hematite is nine times larger than that of feroxyhyte. Hence, several reflections of hematite should be extinct for feroxyhyte. Due to the fact that the *c* axis of hematite is three times larger, only hematite reflections with $l = 3n$ are present for feroxyhyte. In addition, the *c*-glide plane of hematite causes a further extinction rule for hematite of $l = 6n$ for $(00l)$, which is not valid for feroxyhyte. Therefore, only these extinction rules provide an opportunity for unambiguous identification of feroxyhyte. All reflections of powder electron diffraction patterns show only *d* spacings characteristic of feroxyhyte, and also an electron diffraction pattern along the $[010]_{\mathrm{fx}}$ zone clearly violates the extinction of $l = 6n$ for hematite (hem) (see Figure 2). The diffraction spot $(003)_{\mathrm{hem}}$ is weak but clearly present and cannot be an effect of double diffraction. During tilting of the crystal from the $[301]_{\mathrm{hem}}$ zone to the $[601]_{\mathrm{hem}}$ zone, which corresponds to $[1\bar{1}1]_{\mathrm{fx}}$ and $[2\bar{2}1]_{\mathrm{fx}}$ of feroxyhyte, a zone axis of $[401]_{\mathrm{hem}}$ should be clearly visible in the case of hematite, because it contains the $(10\bar{4})$ diffraction spot, one of the strongest reflections of hematite. The absence of this additional zone axis provides evidence for the presence of feroxyhyte (Figure 7).

The atomic structure of hematite is characterized by hexagonally close-packed layers of oxygen, in which 2/3 of the octahedral sites are filled by ferric iron in an ordered manner. In contrast, the unit cell of feroxyhyte corresponds to a primitive cell setting of a close-packed oxygen arrangement, which does not allow an ordered occupancy of any of the octahedral sites. Therefore, feroxyhyte (after the model of Patrat *et al.*, 1983) can be considered as completely disordered hematite, which of course contains some (OH) groups for charge balance. Whether the OH groups are disordered, as in the structural model of feroxyhyte of Patrat *et al.* (1983), or ordered into basal layers, as in the $Fe(OH)_2$-structure type (Parise *et al.*, 2000; Cornell and Schwertmann, 2003), is still not known.

The formation of feroxyhyte occurs in this study only at certain, relatively high Sb(V) concentrations. The necessity of having higher Sb(V) concentrations together with the rapid formation of feroxyhyte indicates a nucleation/crystallization from bulk solution, rather than a solid-state formation of feroxyhyte from hematite by cation disorder. This is supported by considering that Sb-doped hematite remains stable for more than 16 days at 70ºC in aqueous solution without any signs of a transformation to feroxyhyte. The observed apparent

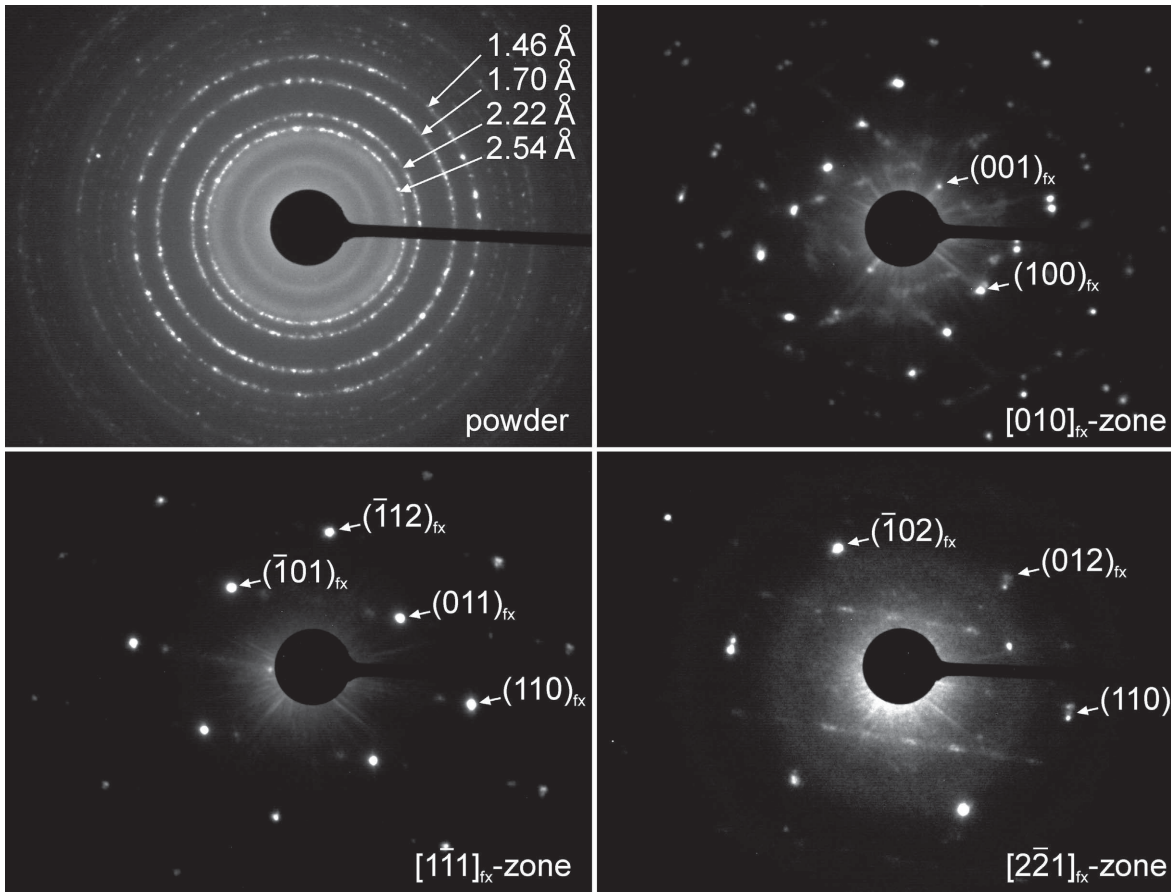

Figure 7. Selected electron diffraction pattern of feroxyhyte. The powder pattern shows the four dominant diffraction lines of feroxyhyte, whereas additional lines of hematite are clearly absent. In the [010] zone pattern, the (001) reflection of feroxyhyte is clearly visible but should be extinct for hematite. The [1$\bar{1}$1] and [2$\bar{2}$1] zone pattern belong to the same crystal tilted by ~18° along the [110] axis.

transition between hematite and feroxyhyte in the XRD patterns is, therefore, considered to be a decreasing hematite signal at increasing Sb(V) concentrations, combined with an increasing feroxyhyte signal, and not a solid-state transformation.

Adsorption or structural incorporation of P(V), As(V), and Sb(V)

During the transformation experiments, P(V) and As(V) showed similar behaviors, consistent with the literature (Das *et al.*, 2011a; Shaw *et al.*, 2005). The formation of hematite was favored over goethite and, at high concentrations of both anions, the transformation was retarded or inhibited. Except for the As(V) adsorption to hematite, the P(V) and As(V) concentrations in the solid transformation product remained below the calculated adsorption capacities, in agreement with previous adsorption studies (Atkinson *et al.*, 1972; Ryden *et al.*, 1977; Barrow *et al.*, 1981; Barron *et al.*, 1988; Torrent *et al.*, 1990; Colombo *et al.*, 1994; Torrent *et al.*, 1994; Arai and Sparks, 2001; Borggaard *et al.*, 2005; Gimsing and Borggaard, 2007; Salazar-Camacho and Villalobos, 2010; Wainipee *et al.*, 2010; Mamindy-Pajany *et al.*, 2011; Zhu *et al.*, 2011).

Transformations in the presence of Sb(V), however, differed strongly from those with P(V) and As(V). During the transformation experiments with Sb(V), goethite was favored over hematite. At higher Sb(V) concentrations, feroxyhyte replaced goethite and hematite. In addition, the solid transformation products feroxyhyte and goethite showed extraordinarily high concentrations of Sb(V).

As most studies deal with the adsorption of contaminants to the surfaces of iron oxides rather than with their structural incorporation, the possibility of a pure adsorption system should be examined. P(V), As(V), and Sb(V) occur in aqueous solution typically as anionic complexes. Between pH 4 and 12, three different pH-dependent species of P(V) and As(V) were distinguished. At pH 4, the dominant species was $H_2(P,As)O_4^-$; at pH 7, $H(P,As)O_4^{2-}$; and at pH 12, $(P,As)O_4^{3-}$. For Sb(V), only one dominant species, $Sb(OH)_6^-$, was

observed over the whole pH range of 4−12 (Brintzinger, 1948; Pitman *et al.*, 1957; Filella *et al.*, 2002). In order to attract and, therefore, adsorb an anionic complex, a positively charged surface was needed, and thus the pH of the solution must have been lower than the point of zero charge (PZC) of the mineral. Feroxyhyte, formed at pH 4 and 7, had a PZC of ~7.5−8 (Borggaard, 1983, Parida *et al.*, 1997). This means that feroxyhyte, under certain conditions, is close to the point of zero charge, but anionic complexes are already attracted by the surface and adsorption is possible. In the experiments carried out, feroxyhyte showed molar Sb:Fe ratios of up to 0.12 (145 mg Sb/g). Can a pure adsorption system explain such high concentrations sufficiently? Unfortunately, no adsorption capacities for feroxyhyte are available in the literature. Under the assumption that one Fe-octahedron on the feroxyhyte surface exposes an area of 0.149 nm^2, as at the goethite (001) face, and a mononuclear monodentate binding of the Sb-octahedra, a maximum of 127 mg Sb/g can be adsorbed to the feroxyhyte surface, which is less than in the feroxyhyte samples. This calculation is based on the specific surface area of the feroxyhyte samples and the chemical surface properties of goethite. As the feroxyhyte structure is still under debate (Drits *et al.*, 1993; Manceau and Drits, 1993) and the occupancy of Fe on the octahedral sites is unclear, the goethite model was considered as a better basis for a rough estimate.

Goethite, on the other hand, which was formed in the experiments at pH 12, showed molar Sb:Fe ratios of 0.03 (44 mg of Sb/g). Considering that the adsorption capacity for goethite calculated after Leuz *et al.* (2006) is ~12 mg of Sb/g, a pure adsorption system is again unlikely. The PZC for goethite is also ~7.2−9.0 (Atkinson *et al.*, 1967; Borggaard, 1983; Gaboriaud and Ehrhardt, 2003; Walsch and Dultz, 2010; Cristiano *et al.*, 2011), which means that at pH 12 the surface of goethite is negatively charged and repels anionic complexes such as $Sb(OH)_6^-$. These findings suggest that mechanisms other than or in addition to pure adsorption take place during the transformation experiments in the presence of Sb(V). These are probably incorporation, but surface precipitation cannot be excluded.

Possible model for the observed findings

The high concentrations of Sb(V) in some of the runs can be explained by adsorption, surface precipitation, or incorporation. As discussed above, the adsorption capacities are insufficient to explain the 'foreign ion' uptake, especially in the case of goethite and feroxyhyte. Surface precipitation is possible, but no evidence for additional phases could be detected by Raman spectroscopy. Therefore, incorporation of Sb(V) into the structures of goethite and feroxyhyte seems to be the most viable explanation for the observations.

Sb(V) is usually coordinated octahedrally in the field of oxygen anions. The ionic radius of Sb(V) is 0.60 Å, very similar to that of 0.55 Å for Fe(III) (Shannon, 1976). In terms of ionic radii, the substitution of Sb(V) for Fe(III) should be easy. Of course, such heterovalent substitution must be coupled with the exchange of other

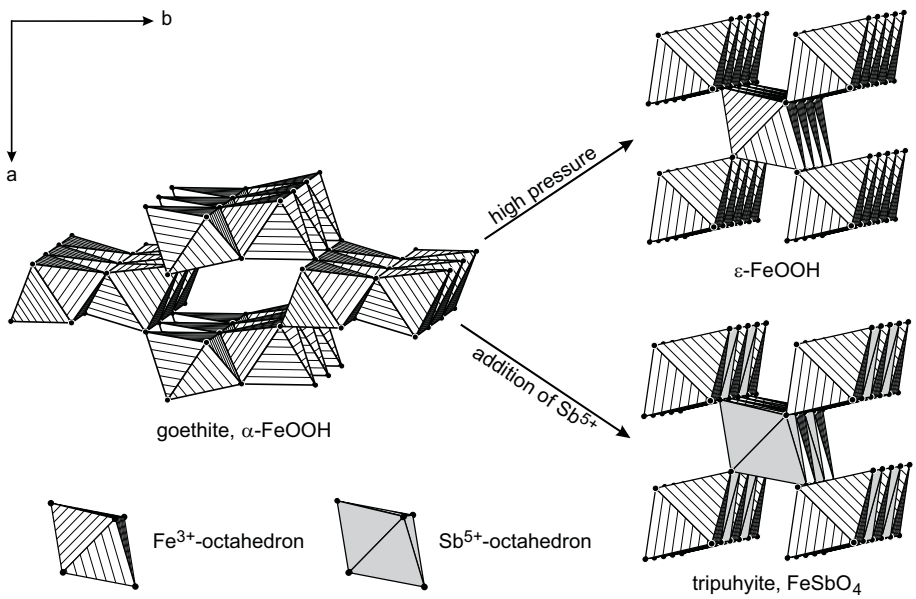

Figure 8. (Left) Structure of goethite (α-FeOOH) consisting of double octahedral chains (*Pbnm* setting). In a high-pressure environment, the tunnels which run parallel to the octahedral chains collapse, forming the denser high-pressure phase ε-FeOOH (upper right). During the Sb(V) → Fe(III) substitution, these tunnels could also collapse, forming the denser tripuhyite structure (lower right). Both ε-FeOOH and tripuhyite are isostructural with rutile.

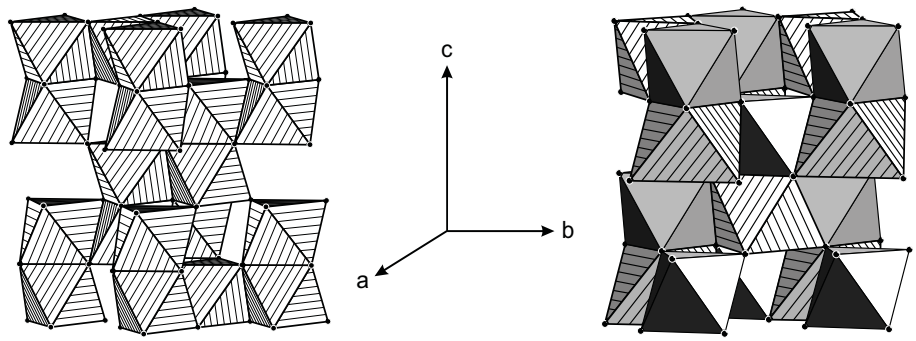

Figure 9. Structures similar to that of hematite (left) can incorporate pentavalent ions. These pentavalent ions cannot occur in close contact with each other because of the strong electrostatic repulsion. In $LiNbO_3$, a superstructure of hematite, the presence of Nb(V) face-sharing octahedra is avoided by monovalent Li^+ octahedra in between, reducing the electrostatic repulsion.

ions. One possibility is the loss of hydrogen concomitant with this substitution:

$$Fe(III) + 2H^+ = Sb(V) \quad (2)$$

Such a mechanism could operate in goethite or feroxyhyte. Here, the loss of some of the H atoms may not be critical to the preservation of the entire structure.

First, the structure of goethite is considered. Goethite consists of [001] double octahedral chains (in the *Pbnm* setting) (Figure 8). The octahedral units in the structure of goethite have the composition $Fe(III)O_3(OH)_3$. The H atoms occupy positions in the tunnels between the double chains. The Fe(III)-Sb(V) substitution would change the composition of the octahedra to $Sb(V)O_5(OH)$ and leave two H positions in the tunnels vacant. The crystal structure of goethite could probably tolerate a certain degree of Sb(V) substitution but would probably collapse if a significant portion of the tunnels remained empty. This mechanism could operate in goethite and account for the Sb(V) incorporation, based on the following crystal-chemical arguments.

The collapse of the tunnels between the double chains in goethite leads to a denser structure with single octahedral chains. Such a structure belongs to the high-pressure polymorph ε-FeOOH (Pernet *et al.*, 1975; Suzuki, 2010) (Figure 8). This phase is isostructural with rutile. Interestingly, tripuhyite, $FeSbO_4$, also has a rutile-type structure (Berlepsch *et al.*, 2003) (Figure 8). Hence, the Fe(III)-Sb(V) substitution in goethite leads to a withdrawal of H atoms, collapse of the tunnels, and a gradual conversion of goethite to tripuhyite on the atomic scale. This transformation from double to single chains can also account for the observation that the crystallinity of goethite worsens with increasing Sb load.

In hematite, coupling of the Fe(III)-Sb(V) with H loss is limited or excluded. Structures derived from that of hematite are capable of incorporating pentavalent cations. The best example is $LiNbO_3$, a superstructure of the hematite structure (Figure 9), with the substitution of 2 Fe(III) for Li^+ + Nb(V). The cations in $LiNbO_3$ are ordered in such a way as to avoid the presence of two Nb(V) ions in two face-sharing octahedra because such an arrangement would lead to a strong electrostatic repulsion. By analogy, by forcing Sb(V) into the structure of hematite, the Fe(III)−Sb(V) repulsion in two neighboring face-sharing octahedra would be too strong. The substitution of 2 Fe(III) for H^+ + Sb(V) seems implausible.

The only way to store a larger amount of Sb(V) in a hematite-related structure is to disorder the cations such that no octahedra share a face with other octahedra. Such octahedra could then be occupied by Sb(V). The disordered variant of the hematite structure is feroxyhyte, δ′-FeOOH, a phase observed in a number of runs.

The presence of tripuhyite in antimony mine tailings was reported in previous studies (Majzlan, 2011; Mitsunobu *et al.*, 2011) though feroxyhyte was not. One possible reason for this is the poor crystallinity as well as the small crystal size of feroxyhyte and the fact that the XRD peaks of hematite and feroxyhyte overlap completely. Feroxyhyte could be identified erroneously as poorly crystalline hematite or hematite could mask the presence of feroxyhyte.

ACKNOWLEDGMENTS

The authors are grateful to Hannes Herzel for his help during the iron oxide syntheses. Thanks also to Dirk Merten, Ines Kamp, Maria Wierzbicka-Wieczorek, and Arkadiusz Wieczorek for their help with ICP-OES, XRD, and SEM, and to Anna Schmidt and Beate Truckenbrodt (all Jena) for BET measurements. In addition, the authors are grateful to two anonymous reviewers and the Editors for their comments and suggestions. This research was funded by the Deutsche Forschungsgemeinschaft (DFG) Research Training Group GRK 1257/1.

REFERENCES

Ackermann, S., Gieré, R., Newville, M., and Majzlan, J. (2009) Antimony sinks in the weathering crust of bullets from Swiss shooting ranges. *Science of the Total Environment*, **407**, 1669−1682.

Álvarez-Benedí, J., Bolado, S., Cancillo, I., Calvo, C., and García-Sinovas, D. (2005) Adsorption-desorption of arsenate in three Spanish soils.*Vadose Zone Journal*, **4**, 282−290.

Ambe, S. (1987) Adsorption kinetics of antimony(V) ions onto α-Fe_2O_3 surfaces from an aqueous solution. *Langmuir*, **3**, 489−493.

Arai, Y. and Sparks, D.L. (2001) ATR-FTIR Spectroscopic investigation on phosphate adsorption mechanisms at the ferrihydrite-water interface. *Journal of Colloid and Interface Science*, **241**, 317−326.

Atkinson, R.J., Quirk, J.P., and Posner, A.M. (1972) Kinetics of isotropic-exchange of phosphate at alpha-FeOOH-aqueous solution interface. *Journal of Inorganic and Nuclear Chemistry*, **34**, 2201−2211.

Atkinson, R.J., Posner, A.M., and Quirk, J.P. (1967) Adsorption of potential-determining ions at the ferric oxide-aqueous electrolyte interface. *The Journal of Physical Chemistry*, **71**, 3, 550−558.

Barron, V., Herruzo, M., and Torrent, J. (1988) Phosphate adsorption by aluminous hematite of different shapes. *Soil Science Society of America Journal*, **52**, 3, 647−651.

Barrow, N.J., Madrid, L., and Posner, A.M. (1981) A partial model for the rate of adsorption and desorption of phosphate by goethite. *Journal of Soil Science*, **32**, 3, 399−407.

Berlepsch, P., Armbruster, T., and Brugger, J. (2003) Tripuhyite, $FeSbO_4$, revisited. *Mineralogical Magazine*, **67**, 31−46.

Blesa, M.A. and Matijevic, E. (1989) Phase-transformations of iron-oxides, oxyhydroxides, and hydrous oxides in aqueous-media. *Advances in Colloid and Interface Science*, **29**, 173−221.

Borggaard, O.K. (1983) Effect of surface-area and mineralogy of iron-oxides on their surface-charge and anion-adsorption properties. *Clays and Clay Minerals*, **31**, 230−232.

Borggaard, O.K., Raben-Lange, B., Gimsing, A.L., and Strobel, B.W. (2005) Influence of humic substances on phosphate adsorption by aluminium and iron oxides. *Geoderma*, **127**, 270−279.

Brintzinger, H. (1948) Die Antimonat-, Antimonit-, Germanat- und Aluminat-Ioden im gelössten Zustand. *Zeitschrift für Anorganische und Allgemeine Chemie*, **256**, 98−102.

Brunauer, S., Emmett, P.H., and Teller, E. (1938) Adsorption of gases in multimolecular layers. *Journal of the American Chemical Society*, **60**, 308−319.

Carlson, L. and Schwertmann, U. (1980) Natural occurrence of feroxyhyte (δ'-FeOOH). *Clays and Clay Minerals*, **28**, 272−280.

Ciobotă, V., Salama, W., Tarcea, N., Rösch, P., Aref, M.E., Gaupp, R., and Popp, J. (2012) Identification of minerals and organic materials in Middle Eocene ironstones from the Bahariya Depression in the Western Desert of Egypt by means of micro-Raman spectroscopy. *Journal of Raman Spectroscopy* **43**, 405−410.

Colombo, C., Barrón, V., and Torrent, J. (1994) Phosphate adsorption and desorption in relation to morphology and crystal properties of synthetic hematites. *Geochimica et Cosmochimica Acta*, **58**, 1261−1269.

Cornell, R.M. and Schwertmann, U. (2003) *The Iron Oxides, Properties, Reactions, Occurrences, and Uses.* Wiley-VCH Verlag, Weinheim, Germany.

Cornell, R.M., Giovanoli, R., and Schindler, P.W. (1987) Effect of silicate species on the transformation of ferrihydrite into goethite and hematite in alkaline media. *Clays and Clay Minerals*, **35**, 21−28.

Cristiano, E., Hu, Y.-J., Siegfried, M., Kaplan, D., and Nitsche, H. (2011) A comparison of point of zero charge measurements methodology. *Clays and Clay Minerals*, **59**, 107−115.

Cudennec, Y. and Lecerf, A. (2006) The transformation of ferrihydrite into goethite or hematite, revisited. *Journal of Solid State Chemistry*, **179**, 716−722.

Das, S., Hendry, J., and Essilfie-Dughan, J. (2011a) Effects of adsorbed arsenate on the rate of transformation of 2-line ferrihydrite at pH 10. *Environmental Science & Technology*, **45**, 5557−5563.

Das, S., Hendry, J., and Essilfie-Dughan, J. (2011b) Transformation of two-line ferrihydrite to goethite and hematite as a function of pH and temperature. *Environmental Science & Technology*, **45**, 268−275.

Diemar, G.A., Filella, M., Leverett, P., and Williams, P.A. (2009) Dispersion of antimony from oxidizing ore deposits. *Pure and Applied Chemistry*, **81**, 1547−1553.

Dörfer, T., Schumacher, W., Tarcea, N., Schmitt, M., and Popp, J. (2010) Quantitative mineral analysis using Raman spectroscopy and chemometric techniques. *Journal of Raman Spectroscopy* **41**, 684−689.

Downs, R. T. and Hall-Wallace, M. (2003) "The American Mineralogist Crystal Structure Database". *American Mineralogist*, **88**, 247−250.

Drits, V.A., Sakharov, B.A., and Manceau, A. (1993) Structure of feroxyhyte as determined by simulation of X-ray diffraction curves. *Clay Minerals*, **28**, 209−222.

Filella, M., Belzile, N., and Chen, Y.-W. (2002) Antimony in the environment: a review focused on natural waters − II. Relevant solution chemistry. *Earth-Science Reviews*, **59**, 265−285.

Fischer, W.R. and Schwertmann, U. (1975) The formation of hematite from amorphous iron(III) hydroxide. *Clays and Clay Minerals*, **23**, 33−37.

Gaboriaud, F. and Ehrhardt, J.-J. (2003) Effects of different crystal faces on the surface charge of colloidal goethite (α-FeOOH) particles: an experimental and modeling study. *Geochimica et Cosmochimica Acta*, **67**, 967−983.

Georgescu, D., Baia, L., Ersen, O., Baia, M., and Simon, S. (2012) Experimental assessment of the phonon confinement in TiO_2 anatase nanocrystallites by Raman spectroscopy. *Journal of Raman Spectroscopy*, **43**, 876−883.

Gimsing, A.L. and Borggaard, O.K. (2007) Phosphate and glyphosate adsorption by hematite and ferrihydrite and comparison with other variable-charge minerals. *Clays and Clay Minerals*, **55**, 108−114.

Grazulis, S., Chateigner, D., Downs, R. T., Yokochi, A. T., Quiros, M., Lutterotti, L., Manakova, E., Butkus, J., Moeck, P., and Le Bail, A. (2009) "Crystallography Open Database − an open-access collection of crystal structures". *Journal of Applied Crystallography*, **42**, 726−729.

Gražulis, S., Daškevič, A., Merkys, A., Chateigner, D., Lutterotti, L., Quirós, M., Serebryanaya, N.R., Moeck, P., Downs, R.T., and LeBail, A. (2012) "Crystallography Open Database (COD): an open-access collection of crystal structures and platform for world-wide collaboration". *Nucleic Acids Research*, **40**, D420−D427.

Guan, X., Dong, H., Ma, J., and Jiang, L. (2009) Removal of arsenic from water: Effects of competing anions on As(III) removal in $KMnO_4$-Fe(II) process. *Water Research*, **43**, 3891−3899.

Hanesch, M. (2009) Raman spectroscopy of iron oxides and (oxy)hydroxides at low laser power and possible applications in environmental magnetic studies. *Geophysical Journal International*, **177**, 941−948.

Hansen, H.C.B., Raben-Lange, R., Raulund-Rasmussen, K., and Borggaard, O.K. (1994) Monosilicate adsorption by ferrihydrite and goethite at pH 3−6. *Soil Science*, **158**, 40−46.

He, Q.H., Leppard, G.G., Paige, C.R., and Snodgrass, W.J. (1996) Transmission electron microscopy of a phosphate effect on the colloid structure of iron hydroxide. *Water Research*, **30**, 1345−1352.

Jambor, J.L. and Dutrizac, J.E. (1998) Occurrence and constitution of natural and synthetic ferrihydrite, a widespread iron oxyhydroxide. *Chemical Review*, **98**, 2549–2585.

Johnston, J.H. and Lewis, D.G. (1983) A detailed study of the transformation of ferrihydrite to hematite in an aqueous medium at 92ºC. *Geochimica et Cosmochimica Acta*, **47**, 1823–1831.

Larsen, O. and Postma, D. (2001) Kinetics of reductive bulk dissolution of lepidocrocite, ferrihydrite, and goethite. *Geochimica et Cosmochimica Acta*, **65**, 1367–1379.

Leuz, A-K., Mönch, H., and Johnson, C.A. (2006) Sorption of Sb(III) and Sb(V) to goethite: Influence on Sb(III) oxidation and mobilization. *Environmental Science & Technology*, **40**, 7277–7282.

Loan, M., Parkinson, G.M., and Richmond, W.R. (2005) The effect of zinc sulfide on phase transformations of ferrihydrite. *American Mineralogist*, **90**, 258–261.

Majzlan, J. (2011) Thermodynamic stabilization of hydrous ferric oxide by adsorption of phosphate and arsenate. *Environmental Science & Technology*, **45**, 4726–4732.

Majzlan, J., Lalinska, B., Chovan, M., Bläss, U., Brecht, B., Göttlicher, J., Steininger, R., Hug, K., Ziegler, S., and Gescher, J. (2011) A mineralogical, geochemical, and microbiogical assessment of the antimony- and arsenic-rich neutral mine drainage tailings near Pezinok, Slovakia. *American Mineralogist*, **96**, 1–13.

Mamindy-Pajany, Y., Hurel, C., Marmier, N., and Roméo, M. (2011) Arsenic (V) adsorption from aqueous solution onto goethite, hematite, magnetite and zero-valent iron: Effects of pH, concentration and reversibility. *Desalination*, **281**, 93–99.

Manceau, A. and Drits, V.A. (1993) Local-structure of ferrihydrite and feroxyhyte by EXAFS spectroscopy. *Clay Minerals*, **28**, 165–184.

Martinelli, A., Ferretti, M., Basso, R., Cabella, R., Lucchetti, G., Marescotti, P., and Buscaglia, V. (2004) Solid state miscibility in the pseudo-binary TiO_2–$(FeSb)O_4$ system at 1373 K. *Zeitschrift für Kristallographie*, **219**, 487–493.

Michel, M.F., Ehm, L., Antao, S.M., Lee, P.L., Chupas, P.J., Liu, G., Strongin, D.R, Schoonen, M.A.A, Phillips, B.L., and Parise, J.B. (2007) The structure of ferrihydrite, a nanocrystalline material. *Science*, **316**, 5832, 1726–1729.

Mitsunobu, S., Takahashi, Y., Utsunomiya, S., Marcus, M.A., Terada, Y., Iwamura, T., and Sakata, M. (2011) Identification and characterization of nanosized tripuhyite in soil near Sb mine tailings. *American Mineralogist*, **96**, 7, 1171–1181.

Nagano, T., Nakashima, S., Nakayama, S., and Senoo, M. (1994) The use of color to quantify the effect of pH and temperature on the crystallization kinetics of goethite under highly alkaline conditions. *Clays and Clay Minerals*, **42**, 226–234.

Paige, C.R., Snodgrass, W.J., Nicholson, R.V., and Scharer, J.M. (1996) The crystallization of arsenate-contaminated iron hydroxide solids at high pH. *Water Environment Research*, **68**, 981–987.

Paige, C.R., Snodgrass, W.J., Nicholson, R.V., Scharer, J.M., and He, Q.H. (1997) The effect of phosphate on the transformation of ferrihydrite into crystalline products in alkaline media. *Water, Air, and Soil Pollution*, **97**, 397–412.

Parida, K.M., Gorai, B., Das, N.N., and Rao, S. B. (1997) Studies on ferric oxide hydroxides. III. Adsorption of selenite (SeO_3^{2-}) on different forms of iron oxyhydroxides, *Journal of Colloid and Interface Science*, **185**, 355–362.

Parise, J.B., Marshall, W.G., Smith, R.I., Lutz, H.D., and Moller, H. (2000) The nuclear and magnetic structure of "white rust"-Fe(OH0.86D0.14)2. *American Mineralogist*, **85**, 189–193.

Patrat, G., de Bergevin, F., Pernet, M., and Joubert, J. (1983) Structure locale de delta-Fe O O H. *Acta Crystallographica B*, **39**, 165–170.

Pernet, M., Joubert, J.C., and Berthet-Colominas, C. (1975) Etude par diffraction neutronique de la forme haute pression de FeOOH. *Solid State Communications*, **17**, 1505–1510.

Pitman, A.L., Pourbaix, M., and de Zoubov, N. (1957) Potential-pH diagram of the antimony-water system. Its applications to properties of the metal, its compounds, its corrosion, and antimony electrodes. *Journal of the Electrochemical Society*, **104**, 594–600.

Ryden, J.C., McLaughlin, J.R., and Syers, J.K. (1977) Mechanisms of phosphate sorption by soil and hydrous ferric oxide gel. *Journal of Soil Science*, **28**, 72–92.

Salazar-Camacho, C. and Villalobos, M. (2010) Goethite surface reactivity: III. Unifying arsenate adsorption behavior through a variable crystal face-site density model. *Geochimica et Cosmochimica Acta*, **74**, 2257–2280.

Schwertmann, U. and Cornell, R.M. (2000) *Iron Oxides in the Laboratory: Preparation and Characterization*, 2nd edition. Wiley-VCH Verlag, Weinheim, Germany.

Schwertmann, U. and Fischer, W.R. (1966) Zur Bildung von α-FeOOH und α-Fe_2O_3 aus amorphem Eisen(lII)-hydroxid III. *Zeitschrift für Anorganische und Allgemeine Chemie*, **346**, 137–142.

Schwertmann, U. and Murad, E. (1983) Effect of pH on the formation of goethite and hematite from ferrihydrite. *Clays and Clay Minerals*, **31**, 277–284.

Shannon, R.D. (1976) Revised effective ionic radii and systematic studies of interatomic distances in halides and chalcogenides. *Acta Crystallographica A*, **32**, 751–767.

Shaw, S., Pepper, S.E., Bryan, N.D., and Livens, F.R. (2005) The kinetics and mechanisms of goethite and hematite crystallization under alkaline conditions, and in the presence of phosphate. *American Mineralogist*, **90**, 1852–1860.

Suzuki, A. (2010) High-pressure X-ray diffraction study of ε-FeOOH. *Physics and Chemistry of Minerals*, **37**, 153–157.

Tighe, M., Lockwood P., and Wilson, S. (2005) Adsorption of antimony(V) by floodplain soils, amorphous iron(III) hydroxide and humic acid. *Journal of Environmental Monitoring*, **7**, 1177–1185.

Torrent, J., Barrón, V., and Schwertmann, U. (1990) Phosphate adsorption and desorption by goethites differing in crystal morphology. *Soil Science Society of America Journal*, **54**, 1007–1012.

Torrent, J., Schwertmann, U., and Barrón, V. (1994) Phosphate sorption by natural hematites. *European Journal of Soil Science*, **45**, 45–51.

Wainipee, W., Weiss, D.J., Sephton, M.A., Coles, B.J., Unsworth, C., and Court, R. (2010) The effect of cruide oil on arsenate adsorption on goethite. *Water Research*, **44**, 5673–5683.

Walsch, J. and Dultz, S. (2010) Effects of pH, Ca- and SO_4-concentration on surface charge and colloidal stability of goethite and hematite – consequences for the adsorption of anionic organic substances. *Clay Minerals*, **45**, 1–13.

Wojdyr, M. (2010) Fityk: a general-purpose peak fitting program. *Journal of Applied Crystallography*, **43**,1126–1128. (reprint)

Zhu, J., Pigna, M., Cozzolino, V., Caporale, A.G., and Violante, A. (2011) Sorption of arsenite and arsenate on ferrihydrite: Effect of organic and inorganic ligands. *Journal of Hazardous Materials*, **189**, 564–571.

(*Received 20 July 2012; revised 24 January 2013; Ms. 695; AE: H. He*)